This is the accepted version of the manuscript:

Matteo Antelmi, Luca Alberti, Adriana Angelotti, Sara Curnis, Andrea Zille, Loris Colombo, Thermal and hydrogeological aquifers characterization by coupling depth-resolved thermal

response test with moving line source analysis*, Energy Conversion and Management 225 (2020)*

Thermal and hydrogeological aquifers characterization by coupling depth-resolved Thermal Response Test with Moving Line Source analysis

Matteo Antelmi[a*], Luca Alberti[a], Adriana Angelotti[b], Sara Curnis[a], Andrea Zille[c], Loris Colombo[a]

[a]Dipartimento di Ingegneria Civile Ambientale, Politecnico di Milano, P.zza L. da Vinci 32, 20133 Milano, Italia.

[c]Dipartimento di Energia, Politecnico di Milano, via Lambruschini 4, 20156 Milano, Italia

[c]GEOZ iSRL, NOI Techpark, via Volta 13, 39100 Bolzano, Italy

corresponding author. Tel. +39 02 2399 6668; e-mail: matteo.antelmi@polimi.it

Declaration of interests

The authors declare that they have no known competing financial interests or personal relationships that could have appeared to influence the work reported in this paper.

CRediT author statement

Matteo Antelmi: Methodology, Software, Validation, Investigation, Data Curation, Writing- Original Draft, Supervision; **Luca Alberti**: Methodology, Conceptualization, Writing- Review & Editing, Supervision, Project Administration; **Adriana Angelotti**: Methodology, Conceptualization, Writing- Review & Editing, Supervision; **Sara Curnis**: Software, Investigation, Data Curation, Writing- Original Draft, Visualization; **Andrea Zille**. Resources, Data curation, **Loris Colombo**. Writing- Original draft preparation

Abstract

In this paper for the first time the Moving Line Source (MLS) model is combined with a depth-resolved Thermal Response Test (TRT). The latter was performed in a heterogeneous and groundwater rich subsoil, composed by a layering of silty sand, medium-fine sand and coarse-medium sand, with a layer of clayey silt separating a shallow aquifer from a deep one.

The temperature evolution in the ground along the vertical axis was analysed with both the standard Infinite Line Source (ILS) and the MLS. The two models lead to similar estimates of the thermal conductivity in those regions of the subsoil

where conduction prevails, while the MLS performs better where a significant groundwater velocity is expected. In these layers, the MLS analysis allow to derive both the thermal conductivity and the Darcy velocity. The MLS results were validated by comparison with a numerical simulation on a multiple-layers ground model developed in MODFLOW/MT3DMS using a constant energy boundary condition. The combined depth-resolved TRT/MLS approach represents an important method for an accurate design of the Ground Heat Exchangers under the presence of groundwater flow.

Highlights

- Moving Line Source analysis applied to depth-resolved Thermal Response Test
- Vertical distribution of thermal conductivity and Darcy velocity achieved
- Thermal and hydraulic properties of layers in good agreement with stratigraphic log
- Layered numerical model validates the MLS results
- Numerical simulation of BHE using ITYPE15 boundary condition

Keywords: Ground Source Heat Pumps, Depth-resolved Thermal Response Test, Advection, Numerical Modelling, Moving Line Source, Groundwater.

Nomenclature

Symbol	Variable	Unit
α	Thermal diffusivity	m^2/s
BHE	Borehole Heat Exchanger	-
C	Volumetric heat capacity of the porous medium or water or pipe	$J/(m^3 \cdot K)$
C^k	Dissolved mass concentration	kg/m^3
C_s	Concentration of the sources or sinks	kg/m^3
c_s, c_w	Specific heat capacity of the solid or water	$J/(kg \cdot K)$
D*	Molecular diffusion coefficient/Thermal diffusion coefficient	m^2/s
D_{ij}	Diffusion-dispersion tensor	m^2/s
Θ	Angle between Darcy velocity and source-probe distance	$\circ$
θ	Volumetric water content of the porous medium	-
GSHP	Ground Source Heat Pump	-
H, h	Hydraulic head	m
K_d	Distribution coefficient	m^3/kg
ILS	Infinite Line Source	-
λ	Effective thermal conductivity of the porous medium	$W/(m \cdot K)$
L	Cell thickness	m
M, N	Total number of data sample	-
MLS	Moving Line Source	-
q	Heat rate per unit length or specific heat rate	W/m
q_s	Volumetric flow rate per unit volume of aquifer representing sources and sinks	$(m^3/s)/m^3$
r	Radial coordinate	m
RMSE	Root mean squared error	°C
ρ_b	Porous medium bulk density	kg/m^3
ρ_s, ρ_w	Density of the solid material or water	kg/m^3
T, T_s, T_0	Temperature, temperature of the source or undisturbed ground	°C
T_{ILS}, T_{MLS}, $T_{MODFLOW}$, T_{meas}	Temperature achieved by Moving Line Source, or Infinite Line Source or MODFLOW approaches or measured data	°C

T_{abs_res}	Absolute residual mean error of temperature	°C
t	Time	s
v_i, v_D	Seepage velocity and Darcy velocity	m/s
x_i, x_j	Space coordinates along directions i and j	m
z	Depth	m

1. Introduction

Ground-Source Heat Pumps (GSHP) are highly efficient heating and cooling systems, mainly diffused in Europe [1] and North America, and recently increasing worldwide [2–4]. By means of closed-loop Ground Heat Exchangers (GHE) they exploit the low-depth ground as a heat source or sink, namely a "shallow geothermal energy" in principle available everywhere. Clearly, GSHP application does not appear economically feasible and operationally efficient in cities with tropical climates, where the ground temperature is relatively high and a significant imbalance between cooling and heating demand exists [5].

Influence of groundwater flow on the BHE performances. Whenever a regional groundwater flow is present, the GHE performance is generally enhanced because heat transfer in the ground occurs by both conduction (related to the ground thermal conductivity and thermal diffusivity) and advection (related to the groundwater velocity). The Péclet number is often used to quantify the relative importance of advection over conduction and thus to identify when groundwater influence on the GSHP performance is relevant. The characteristic Péclet length can be taken as either the soil mean grain size [6], the borehole diameter/radius [7,8] or even the spacing among boreholes [9].

The influence of groundwater flow on the Borehole Heat Exchangers (BHE) operation was studied by several authors, mostly by numerical modelling [7–15] and by analytical modelling [16,17], more rarely by field experiments [18].

Fuji et al. [7] simulate the behaviour of a large-scale borefield in the Akita Plain (Japan) under the groundwater velocity of $1.4 \cdot 10^{-4}$ m/day for 50 years. They find that, if the system is used for heating only or is subjected to a large imbalance between heat extraction and injection, upstream boreholes show higher heat exchange performances than downstream ones. Therefore, they suggest taking into account groundwater flow effect to optimise the borefield operation, implementing more heat storage in downstream boreholes.

Hein et al. [12] study numerically the long-term operation of a GSHP and show that groundwater flow as well as using the system also for cooling are beneficial to the energy recovery and to the heat pump efficiency.

Wang et al. [18] find that a strong groundwater advection enhances the thermal performance of the BHE. The enhanced effect depends to a great extent on the distribution and thickness percentage of the ground layer with the greatest groundwater flow. In their case, when the total thickness of coarse sand and gravel layer as a percentage of the borehole depth was 10.6%, the heat injection and heat extraction of the BHE were enhanced on average by 10 % and 13 %, respectively, compared with the case without groundwater flow.

Casasso and Sethi [19] observe that the influence of the Darcy velocity on the performances of the system is much stronger than the variation induced by different saturated thicknesses. This means that the contribution of the advection can be taken into account, but precise values are needed to avoid undersized design.

Samson et al. [20] assess the impact of the groundwater flow velocity and angle on the economics of a project of borehole field, by considering both the initial and the annual operation costs. They find that the project is more sensitive to the groundwater flow velocity than to the angle. Moreover, they show that passing from $Pé = 10^{-4}$ to $Pé = 10^{-1}$ with a ground thermal conductivity equal to 1.5 W/(m·K) decreases the total cost by 5.8%. Finally, the total cost of a borefield operating in off-design conditions is quantified, highlighting the importance to know both thermal conductivity and Darcy velocity in the design phase.

The seasonal fluctuations of the hydrothermal properties in the soil are taken into account in [21], while in [22] the impact of the thermally induced water flow and convection on Soil-Borehole Thermal Energy Storages (SBTES) is demonstrated. Groundwater flow is proved to be beneficial for mitigating the thermal drift in the ground induced by a seasonally unbalanced operation of the GSHP [23], and thus advective heat flux should be taken into account in the ground energy balance together with the ground surface heat flux [24].

Environmental issues related to the impact of the BHE on the groundwater quality are analysed by [25], who simulate in a test facility the release of the antifreeze additive polypropylene-glycol, observing the leaching of the main heavy metals. The Authors also investigate the role of the BHE grouting in changing the hydraulic conditions of aquifers, because defects and voids in the grout may increase the hydraulic conductivity along the boreholes, and quantify the magnitude of the inter-aquifer flux, assuming typical hydraulic parameters of the alluvial aquifer of Padana Plain (N Italy).

Standard TRT as a mean to know thermal conductivity. The design of the BHE typically requires the knowledge of the ground thermal conductivity. Thermal Response Test (TRT) is a well-known experimental procedure that allows to obtain this crucial parameter on site, together with the borehole thermal resistance and the ground undisturbed temperature [26–32]. In the standard TRT an external source provides a constant heat rate to the fluid that is circulated at a given flow rate in a test BHE typically for 2-3 days. The variation with time of the inlet and the outlet fluid temperature is monitored and, by inverse modelling of the mean fluid temperature profile, the ground and borehole relevant parameters are estimated. The most popular model used to interpret the TRT data is the Infinite Line Source (ILS) analytical model [33], representing the BHE as an infinite linear source embedded in an infinite homogeneous medium with uniform initial temperature, where heat transfer happens only by conduction.

Influence of groundwater on TRT. The presence of a regional groundwater flow affects the TRT results. In [9] a finite elements numerical model of groundwater flow and heat transfer is used to simulate a standard TRT for increasing Darcy velocities. With respect to the null velocity case, the fluid thermal response features a steady state regime. As the groundwater velocity increases, the time to reach steady state and the temperature asymptotic value decrease. According to Witte [34] a clear indication of the groundwater presence in a TRT can be obtained by plotting the estimate of the thermal conductivity as a function of the measuring time: as more data are added, the thermal conductivity tends to

increase and often a stable estimate cannot be reached. Signorelli et al. [35] use a numerical model to study the effect of soil heterogeneities and groundwater flow on the TRT results. By assuming the borehole diameter as the characteristic length in Péclet number, they show that the ILS analysis returns an effective thermal conductivity, combining conduction and advection, that overestimates the pure thermal conductivity by 7% at Pé ~ 1.7 and by 17% at Pé ~6.8. Raymond et al. [36] show that using a numerical groundwater flow model to analyse a TRT with significant groundwater flow allows to distinguish the effects of hydraulic and thermal properties and therefore provides additional information for designing systems, compared to the approach that combines conduction and advection in a single effective conductivity value. In a recent study by [37] it is shown that the seasonal variations of the groundwater level can affect the thermal conductivity estimate in a TRT performed on a shallow BHE, leading to different results for tests executed in different times of the year.

In order to study groundwater flow influence on TRT and to understand how to obtain the key parameters affecting both conduction and advection heat transfer, an alternative to numerical modelling is represented by laboratory scale experiments in so-called sand boxes [38–40]. Compared to field experiments, they allow to control and vary the ground thermal properties and the water flow parameters. Results achieved at the sand box scale can easily be brought to the field scale if a heat transfer similarity approach is adopted [40].

The MLS to analyse standard TRT under groundwater flow. Concerning analytical models suitable to analyse a TRT influenced by groundwater flow, some authors proposed and tested the application of the Moving Line Source (MLS). The MLS [41,42] generalizes the ILS by considering an infinite homogeneous porous medium surrounding the linear source, with a uniform horizontal fluid flow. In [43], the MLS is compared with the groundwater g-functions and with a mass-transport model in the analysis of a TRT. It is found that the mass-transport solution yields the more realistic results, especially in cases with high groundwater flow where thermal dispersivity is an important parameter. Wagner et al. [44] show that inverse modelling of the TRT through the MLS tends to underestimate the true Darcy velocity because it disregards the borehole volume, where the grouting with a negligible hydraulic conductivity inhibits the water flow. Therefore, they calculate by numerical simulations a correction factor to be applied to the velocity value derived from TRT fitting in order to obtain the true velocity. In [45] the MLS analysis is applied to two real TRT data, highlighting the issue of multiple solutions. The Authors find that while in the advection-dominated case physical considerations driven by the general knowledge of the hydrogeological conditions of the site can help to identify the more realistic solution, in the case where conduction and advection compete the MLS analysis may not be successful in identifying the Darcy velocity. Chae et al. [46] propose a practical method for the simultaneous determination of both the groundwater velocity and the effective thermal conductivity of soil by using the MLS theory, by applying the radius of an equivalent single pipe instead of the borehole radius to the MLS model, under the conditions in which the borehole is filled by the

surrounding porous soil with the groundwater flow. The method is applied to a TRT carried out in Kazuno City, Japan, where alluvial gravel deposits were buried in a valley to a depth of over 100 m, resulting in a Darcy velocity equal to 120 m/y and a thermal conductivity of 4.7 W/(m·K). In all these papers [43–47], since the MLS model is applied to a standard TRT where just inlet and outlet fluid temperature are measured, only depth-averaged heat transfer properties of the ground can be obtained, namely any subsoil heterogeneity is neglected.

Distributed TRT. The evidence of groundwater impact on conventional TRT recently stimulated the development of innovative TRT including groundwater from their design. In [47] the concept of a combined Hydro/Thermal Response Test to simultaneously estimate the ground thermal and hydraulic properties is introduced and numerically studied. The setup uses three temperature sensors set around a heating cable in a borehole, to detect the horizontal temperature gradient, which is sensitive to the water flow velocity modulus and direction. A similar approach is applied by [48] in a TRT in Aachen, where two Temperature Sensor Modules are attached to a BHE at depths of 82 and 94 m, where groundwater flow is expected. Each TSM consists in 48 probes on a cylindrical tube, measuring the temperature distribution at the exterior of the BHE. They obtain a groundwater flow of 0.4 m/day in the NW direction and a negligible velocity at 82 m and 94 m depths, respectively.

Depth-resolved TRT are advanced tests where the temperature variation with time is monitored along the BHE, allowing the determination of local ground thermal conductivities and borehole thermal resistances. According to [49] depth-resolved tests can be distinguished in Distributed Thermal Response Tests (DTRT) and Enhanced Thermal Response Tests (ETRT). While in DTRT heating is supplied by the circulating heating fluid as in conventional TRT, ETRT use a current-carrying wire inserted in the borehole (inside or outside the U-pipe) as the heating source. A continuously distributed temperature profile can be detected with either a fiber optic cable [50–52], or a wireless spherical sensor moving at the same velocity of the fluid [53], the latter being possible only in DTRT. The temperature log along the vertical axis can even be discrete, when plain temperature probes are positioned at given distances along the heating cable [54] or in a dedicated pipe inside the borehole [55].

Content and aim of the present paper. Although a depth-resolved TRT could allow in principle to determine local values of both thermal conductivity and Darcy velocity in water saturated layers, no research in this regard has been reported yet [49].

Therefore, this paper presents an original approach combining for the first time a depth-resolved Enhanced Thermal Response Test with the Moving Line Source analysis. The main novelty of the paper lies in the fact that, contrary to previous applications of the MLS to TRT [43–46], the aquifer is treated as heterogeneous and, thanks to the ETRT procedure, it is possible to derive not only the average thermal conductivity and Darcy velocity, but specifically the vertical distribution for both. This approach would provide the necessary detailed inputs for an accurate design of BHE

9

operating in heterogeneous aquifers with a significant groundwater flow. For instance, it would couple naturally with the BHE design method developed by Hu [56], which can consider the effect of groundwater flow in multiple-layer hydrogeological structure.

2. Methodology

A depth-resolved TRT, specifically an Enhanced TRT (ETRT), was carried out in Lombardy Region (Italy), in a groundwater rich area at the Lodi Experimental Didactic Zootechnical Centre (EDZC). Through this procedure, vertical logs of the unperturbed and the perturbed temperature from the ground level to 60 m depth were achieved. The temperature variations with time along the BHE were then interpreted with analytical solutions, at first with the Infinite Line Source (ILS), taken as the standard TRT interpretation, and then with the Moving Line Source (MLS), which was applied to a depth-resolved TRT for the first time. The outcomes of the two approaches were compared and discussed. At last a validation of the MLS results was performed against a numerical model developed through MODFLOW and MT3DMS codes, featuring the ITYPE15 boundary condition for heat source simulation.

2.1 Field case description

The ETRT was carried at the EDZC, used by the Veterinary Faculty of the Università degli Studi di Milano to perform experiments and researches in the food and veterinary field. In this area a GSHP system was designed and realized in 2014 to provide heating, cooling and ventilation to a post-weaning piglet room, located in one of the sheds of the EDZC [57]. The ground heat exchanger is composed of 5 BHEs (Figure 1) 60 m deep. The borefield encompasses also 7 piezometers and, during the installation of the GSHP, several field tests (i.e. geognostic survey, hydraulic pumping test, hydraulic slug test and standard TRT) were performed to investigate the geology of the subsoil and the hydraulic and thermal parameters of the aquifer.
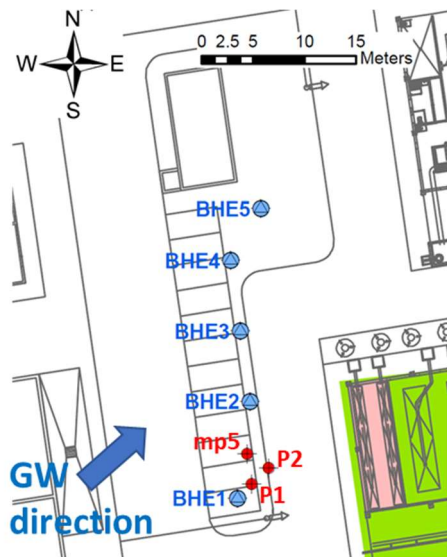
Figure 1 – Case study area in the EDZC: the post-weaning piglet room (pink and included in the shed, marked as green), the BHE (from BHE n.1 to n.5), the micro-piezometer (mp5), the piezometers (P1 and P2) and the groundwater flow direction at local scale.

Based on literature [57–60], the hydrogeological characteristics of the subsoil are approximately known. A specific geognostic survey carried out in the proximity of BHE 1 (Figure 1) revealed the exact layering of lithologies along the depth (Figure 3 a): in the first 18 m a sequence of silty sand and sandy is followed by nearly 10 m of medium sand and gravel; between 30 and 33 m a layer of clayey silt (that locally separates the shallow aquifer from the deep one) is present and followed by coarse-medium sand with gravel until 45 m; from 45 to 60 m a layer of medium-fine sand is revealed.

The hydraulic tests (namely the pumping test and the slug test) allowed to estimate the hydraulic conductivity values of the aquifer and the direction of groundwater flow was determined as from SSW to NNE [57].

The standard TRT executed in the BHE 4 (Figure 1) was interpreted in [61] through analytical and numerical approaches, resulting in some inconsistencies in the evaluation of the thermal conductivity value related to the choice of the interpreting model. In specific the results of ILS and MLS solutions were not in accordance with the results of numerical modeling and experimental data: thermal conductivity ranged between 0.53 and 3.84 W/(mK). Therefore, these differences suggested to study in detail the stratigraphy of the subsoil, evaluating the behaviour of different non-uniform layers by means of a depth-resolved TRT.

2.2 ETRT apparatus and procedure

In order to carry out the ETRT, some preliminary field operations were needed: the GSHP was turned off, an amount of soil was partially removed in the proximity of BHE 5 and the connections among the BHEs were interrupted in order to connect the new TRT apparatus. BHE 5 is a single HDPE U-pipe with a diameter equal to 40 mm and a thickness of 3.7 mm; the perforation diameter is about 12.7 cm and the borehole was originally backfilled with thermally enhanced grout. To perform the ETRT, the GEOsniff instrumentation developed by enOware GmbH was used. Once the BHE was identified and the inlet/outlet pipes were open and free from constraints, a heating cable was inserted and connected to an electric control unit setting a specific heat rate $q = 15.6$ W/m.

Subsequently, 5 GEOsniff Measurement Pig sensors (aluminium spherical sensors, 20 mm diameter and accuracy of 0.05 °C according to the company) were inserted inside the inlet U-pipe at different times. They were not located at fixed depths along the vertical of the BHE, but were dropped by gravity from the top to bottom of the U-pipe into the BHE. Falling by gravity, each sensor measured temperature and pression values along the vertical profile from the ground level down to the bottom at 60 m (Figure 2 a). Measuring the pressure inside the water column allows to derive the depth of the sensor.
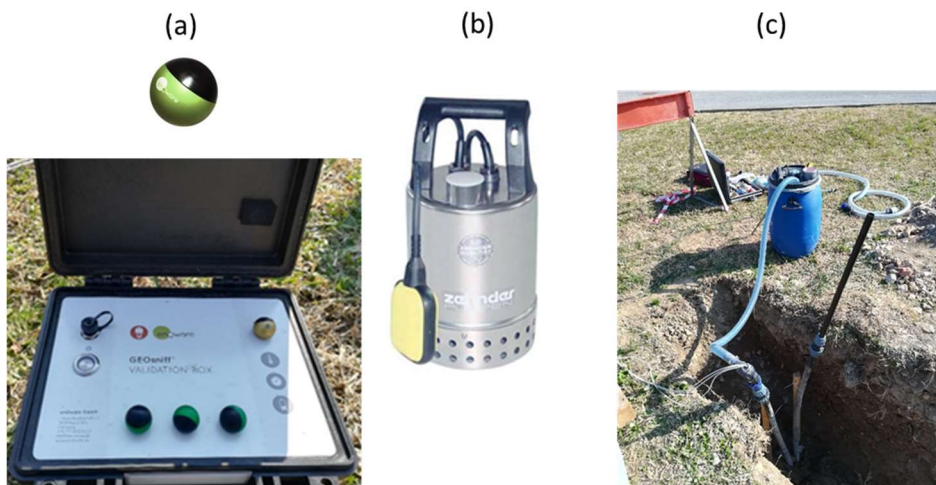

Figure 2 – (a) GEOSniff Measurement Pig sensors and box for data download; (b) hydraulic submersible pump; (c) TRT apparatus linked to BHE n.5 in EZDC.

Before turning on the heating cable, the first sensor was inserted in order to evaluate the unperturbed temperature vertical profile of the ground. After the cable switch on, the times for the insertion of the other 4 probes were automatically chosen by the GEOsniff tool. As Table 1 shows the measurement frequency is higher in the first 24 h when the temperature increase is expected to be larger. The descent in the U-pipe branch down to 60 m was about 5 minutes. Considering that

the sampling frequency was set to 1 Hz the vertical resolution of the measurements was approximately 20 cm, that can be considered as an indication of uncertainty along the depth; the accuracy of electrical power measurement was equal or less than 2 %.

Heating cable status	Time (h)	GEOsniff Measurement Pig
OFF	0	Sensor n.1
ON	3	Sensor n.2
ON	7	Sensor n.3
ON	24	Sensor n.4
ON	96	Sensor n.5

Table 1

Time instants of the 5 sensors insertion in the BHE-5.

After 4 days the heating cable was turned off and the ETRT ended, therefore the 5 sensors were recovered from the BHE using a hydraulic submersible pump placed in the barrel (Figure 2 b and c), and placed on the validation box to download the recorded data of temperature and pression.

2.3 ETRT results

The temperature profiles along the depth measured at the different times are reported in Figure 3 b. In the first 5 meters from the ground level, the thermal profiles were strongly influenced by the external air temperature and the solar radiation, since the first 2 meters of BHE were directly exposed to the outdoor environment because of the excavation needed around U-pipes. Therefore, the data in the range 0-5 m were disregarded.

The thermal response of each subsoil layer is expected to be related to the different thermal and hydraulic properties. Hence, comparing the vertical thermal profile of the aquifer with the lithologies revealed in the stratigraphic log (Figure 3 a) allowed to achieve the thermal response of each subsoil in relation to a controlled thermal excitation.
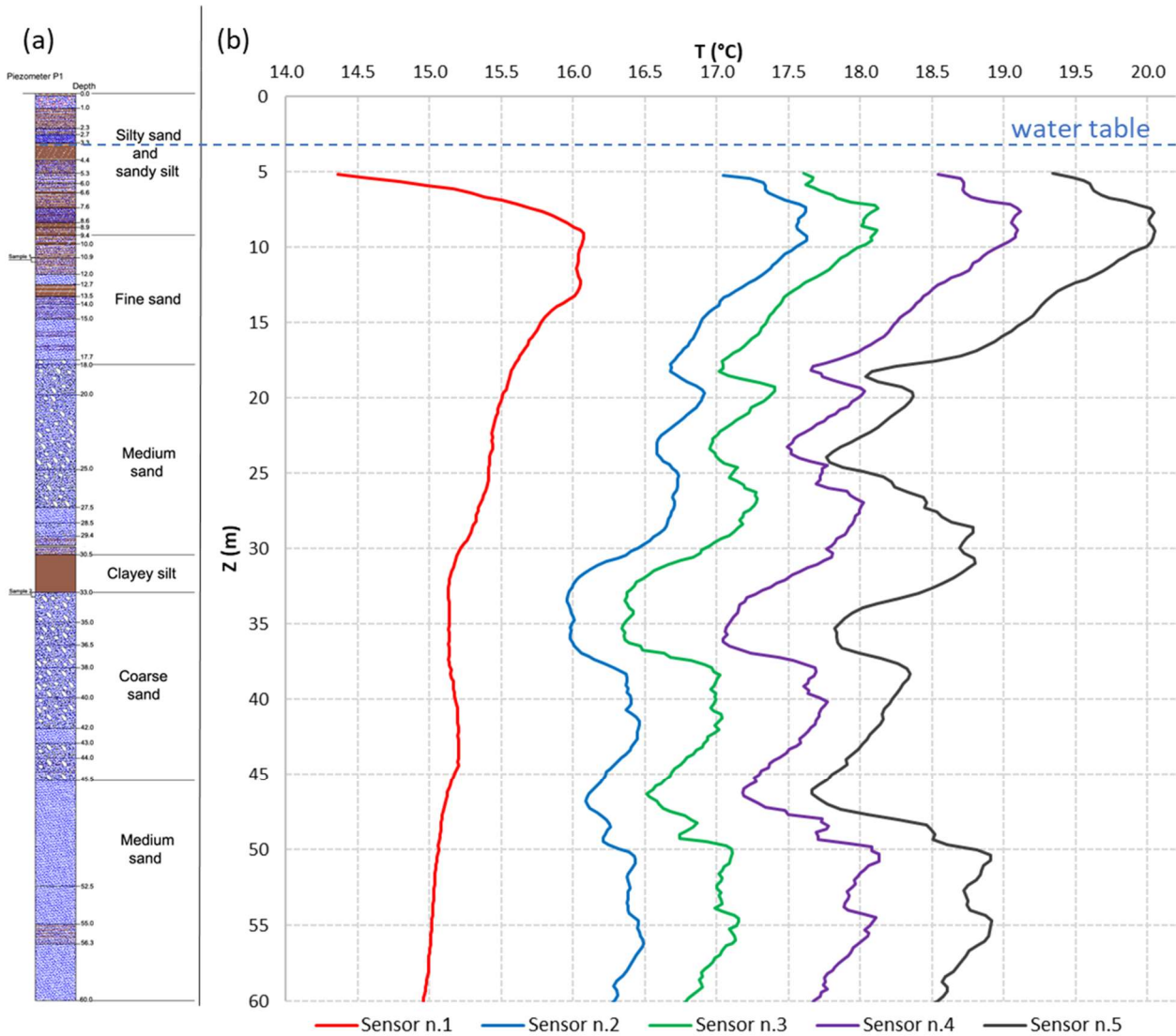
Figure 3 – (a) Stratigraphic log inferred by means of the preliminary geognostic survey in piezometer P1; (b) Thermal log recorded at different depths for the 5 sensors released at 5 different moments during the ETRT.

The unperturbed aquifer temperature corresponds to the red curve in Figure 3 b, whereas the remaining 4 profiles, measured during the heat injection, are increasingly higher with temperatures and heat transfer influenced by each different lithology.

As an example, in Figure 4 the temperature variation with time with respect to the initial value at the depths of 25 m (medium sand), 32 m (clayey silt) and 37 m (coarse medium sand) is reported, together with the variation of the average temperature in the 5-60 m range. Clearly the temperature profiles are more simplified than in a standard TRT where the time resolution is almost continuous. It can be noticed that at 25 m the temperature rise at the beginning is steeper and the temperature increase at the end of the ETRT is lower and almost steady, possibly indicating both high conductivity and groundwater velocity. In turn at 32 m and 37 m a steady state regime is not reached after 96 h. At these depths the

derivative of the temperature with time is initially similar, but between 7 h and 24 h the temperature profile at 37 m gets smoother, probably due to advection. Moreover, the final temperature increase at 32 m is the highest, in agreement with the expectation of a negligible groundwater velocity in an almost impermeable layer.
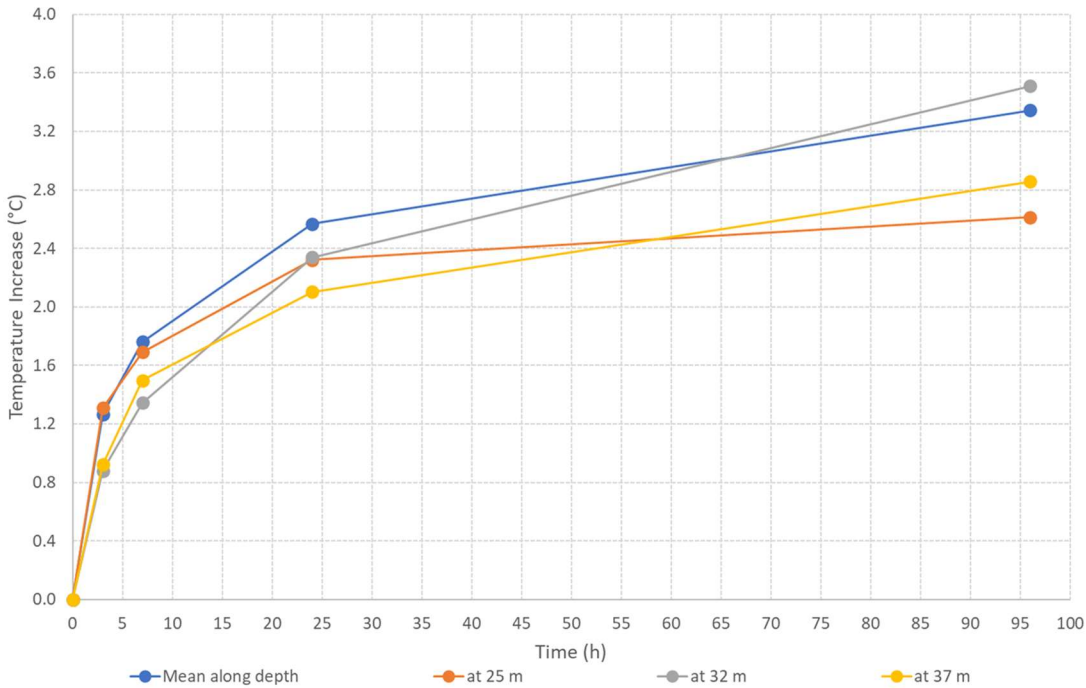

Figure 4 – ETRT results: temperature increase along the entire depth of the BHE (mean value in blue line), at 25 m depth (medium sand), at 32 m depth (clayey silt) and at 37 m depth (coarse medium sand line).

2.4 ETRT interpretation

The ETRT data were firstly interpreted with two analytical models, the Infinite Line Source (ILS) and the Moving Line Source (MLS) and then with a numerical model. The equations and the details of each model are outlined below.

2.4.1   Analytical approach: Infinite Line Source

The most used procedure to evaluate a TRT is based on the Infinite Line Source theory (ILS). According to this approach, the borehole heat exchanger is approximated as an infinite line source in a homogeneous, isotropic and infinite medium, injecting or extracting a constant heat rate per unit length (q), considering only the conductive component of heat transport. The temperature distribution around the infinite line source, as a function of the radial distance and the time, is the following [45]:

$$T_{ILS}\,(r,t) - T_0 = \frac{q}{4\pi\lambda}\int_{\frac{r^2}{4\alpha t}}^{\infty}\frac{e^{-u}}{u}\,du = \frac{q}{4\pi\lambda}E_i\left[\frac{r^2}{4\alpha t}\right] \qquad (1)$$

where T_0 is the undisturbed medium temperature, λ and α are the thermal conductivity and thermal diffusivity of the medium respectively, and E_i is the exponential integral function. In a standard TRT, equation (1) is evaluated at the borehole radius and, by means of a simple thermal network, it is used to derive the mean fluid temperature. In turn, in this case it was evaluated at the distance between the heating cable and the temperature probe, namely the distance between the U-pipe legs. For every depth z_i the root mean squared error between the analytical profile in equation (1) and the measured profile was evaluated:

$$RMSE_{ILS}(z_i) = \sqrt{\frac{\sum_{k=1}^{M}[T_{ILS}(t_k) - T_{meas}(z_i,t_k)]^2}{M}} \qquad (2)$$

Then, by means of the *fminsearch* algorithm in Matlab, the thermal conductivity value λ_i minimizing the $RMSE_{ILS}(z_i)$ was identified. As already explained in subsection 2.2, the ETRT was executed on an existing BHE; therefore, the distance between the U-pipe legs was treated as an uncertain parameter, possibly varying along the BHE depth, between a minimum of 4 cm and a maximum of 8 cm. In addition, the thermal capacity of the medium, included in the thermal diffusivity in equation (1), was considered variable between 2.2 MJ/(m³·K) and 3.4 MJ/(m³·K), on the basis of the literature values for each lithography. Therefore, the fitting process included a sensitivity analysis to the thermal capacity and to the source-probe distance. At first, the source-probe distance was set to 6 cm and the fitting was performed by varying the thermal capacity in the mentioned range with a step equal to 0.1 MJ/(m³·K). This allowed to set the thermal capacity of each layer to the one corresponding to the minimum $RMSE(z_i)$, namely to the best fit. Secondly, the source-probe distance was varied in the given range with a step of 0.5 cm around 6 cm and a larger step of 1 cm near the ends of the range. This allowed to find the most likely source-probe distance and thermal conductivity of the layer as the ones associated to the best fit.

2.4.2 *Analytical approach: Moving Line Source*

According to the Moving Line Source model [41,42], an infinite line source moves with a certain velocity in the x direction or, equivalently, the porous medium moves with the same velocity with respect to the source. The temperature increase in the ground is calculated in polar coordinates by the following expression:

$$T_{MLS}\,(r,\theta,t) - T_0 = \frac{q}{4\pi\lambda}\exp\left(\frac{\rho_w c_w v_D r\cos\theta}{2\lambda}\right)\int_0^{\frac{(\rho_w c_w v_D)^2 t}{4C\lambda}}\frac{1}{u}\exp\left\{-u - \frac{(\rho_w c_w v_D)^2 r^2}{16\lambda u}\right\}du \qquad (3)$$

where ρ_w and c_w are the density and the specific heat of water respectively, v_D is the Darcy velocity, Θ is the groundwater flow direction, λ and C are the thermal conductivity and the volumetric heat capacity of the medium. In this study, equation (3) was used to evaluate the temperature increase at the source-probe distance. As for the ILS analysis, the root mean squared error between the MLS profile and the measured profile was calculated:

$$\mathrm{RMSE_{MLS}}(z_i) = \sqrt{\frac{\sum_{k=1}^{M}[\mathrm{T_{MLS}}(t_k) - \mathrm{T_{meas}}(z_i, t_k)]^2}{N}} \tag{4}$$

and minimized assuming both the layer thermal conductivity λ_i and the Darcy velocity v_{Di} as fitting parameters. Similarly to the ILS case, a sensitivity analysis to the layers thermal capacity and to the source-probe distance was carried out. In addition, the angle Θ between the groundwater direction and the source-probe direction was considered an uncertain parameter. As already mentioned in subsection 2.1 the piezometric tests carried out during the design of the GSHP system in November 2013 allowed to estimate that the groundwater flow is from SSW to NNE. However, the orientation of the line joining the U-pipe legs is not known and, moreover, it may even change along the vertical. Starting from the value of 90°, the angle was varied between 0° and 180° with a step of 45°.

2.4.3   Numerical approach: MODFLOW/MT3DMS

In order to validate the MLS results and thanks to the analogy between solute transport and heat transport equations, a numerical model was implemented using the codes MODFLOW-2000 [62] and MT3DMS [63]. MODFLOW, developed by U. S. Geological Survey, is the most common code used to simulate groundwater flow in a three-dimensional porous medium. It solves numerical models, which suppose a horizontal and vertical discretization of the domain into homogeneous or unitary elements, i.e. cells, where the set of numerical equations are applied. MT3DMS is a modular three-dimensional multispecies transport model for the simulation of advection, dispersion and chemical reactions of contaminants in groundwater systems. It is a code used to simulate the concentrations changes of contaminants or the heat transport in a three-dimensional porous medium. Both the codes can solve the groundwater flow and transport equations using the finite differences method.

The partial differential equation describing the fate and transport of contaminants of species k in three-dimensional, transient groundwater flow systems, disregarding chemical reactions, can be written as follows [13,63]:

$$\left(1 + \frac{\rho_b K_d}{\theta}\right)\frac{\partial(\theta C^k)}{\partial t} = \frac{\partial}{\partial x_i}\left(\theta D_{ij}\frac{\partial C^k}{\partial x_j}\right) - \frac{\partial}{\partial x_i}(\theta v_i C^k) + q_s C_s \tag{5}$$

Even though MT3DMS was designed to simulate solutes transport, thanks to analogies between solute and heat transport processes, the governing equations for solute transport in the subsurface can be represented by similar differential

equations for heat transport. The partial differential equation for heat transport in transient groundwater flow systems solved by MT3DMS can be written as follows [63,64]:

$$\left[1 + \frac{\rho_b K_d}{\theta}\right]\frac{\partial(\theta T)}{\partial t} = \frac{\partial}{\partial x}\left(\theta[D^* + D_{ij}]\frac{\partial T}{\partial x_j}\right) - \frac{\partial}{\partial x_i}(\theta v_i T) + q_s T_s \qquad (6)$$

For the aim of the work, the Sink & Source Mixing Package (SSM package), used to model the last right term of equation 6, is the most important aspect. This term generally represents the contaminant mass entering or leaving the domain. Hence, for heat transport, it is needed to take into account the energy entering or leaving the domain. This term allows us to simulate the constant heat rate injected into the ground by the cable during the ETRT, that is 15.6 W/m along the 60 m depth. In specific, to be consistent with the dimensions relating the contaminant and heat transport, the quantity "mass per unit time and unit volume" ($kg/(s \cdot m^3)$) is equivalent to the quantity "energy per unit time and unit volume" ($J/(s \cdot m^3)$). Thus, energy input/extraction is stated similar as a mass load per unit volume of aquifer.

The source and sink term for heat transport is implemented in MT3DMS in the SSM and the type of source must be set to a mass-loading source, assigning the ITYPE parameter equal to 15 [13,65]. In the SSM package an input value of temperature multiplied by volume flow rate $q_s T_s$ ($K \cdot m^3/s$) has to be assigned for each cell of the source, calculated as:

$$q_S T_s = \frac{q \cdot L}{\rho_w c_w} \qquad (7)$$

where q is the specific heat rate along the cell vertical thickness (W/m) and L is the cell thickness (m).

A numerical model, described below, was implemented to simulate the ETRT. The model describes a layered porous medium domain (200 m x 60 m x 79 m) with a vertical finite line source 60 m long placed in the centre of the domain and equivalent to the heating cable (Figure 5). Concerning the horizontal discretization, the grid was divided into 54 rows and 79 columns of variable size and in specific, from cells with 10 meters side to a central cell with side equal to 0.44 cm. MODFLOW reproduces elements with a square or rectangular grid, so it is not possible to implement circular elements, such as the heating cable. The diameter of the heat exchanger wire was 4.95 mm (section equal to 19.2 mm^2) and has circular geometry, therefore it was implemented with an equivalent square cell of side 4.4 mm. Then, 63 layers of different thickness were defined to reproduce a total depth of 78.81 m; the layers from 1 to 61 are 1 m thick, while the layers 62 and 63 have a thickness of 5 m and 13 m respectively. The real stratigraphy (Figure 3) was reproduced, although simplified, with a local shallow aquifer (layers 1-31) separated by a clayey silty layer (layers 32-33) from a deep one (layers 34-63). The BHE was located in layers 1-60, so the last two layers represent the subsoil without the U-pipe to avoid the influence of the bottom no-flow boundary conditions. The model domain was rotated in order to parallelize the rows with the flow direction. Then at the left and right sides of the model, two boundary conditions of hydraulic constant heads were assigned, reproducing a gradient equal to 0.4% for the shallow aquifer and 0.25% for the deep one. At both

boundaries, the undisturbed temperature of the aquifer was assigned, differentiating as function of the depth and inferred form the descent of sensor n.1 (see "Initial_Temp" in Table 2).
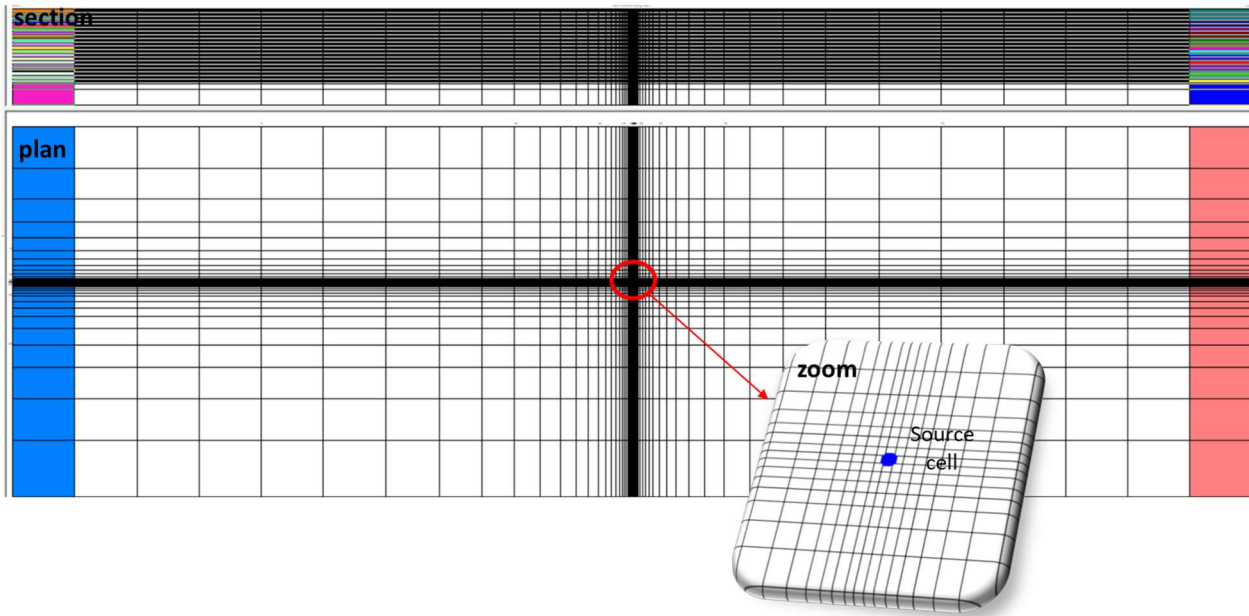

Figure 5 – Plan and section (above) views of the model domain and plan zoom on the source cell with in evidence the grid refinement at centre; left side (blue) and right side (orange) the constant head boundary conditions.

At last, two different numerical models were created: the thermal and hydrogeological properties of model 1 (named M1) were derived from the interpretation of the standard TRT presented in Ly's thesis [61], whereas the properties of model 2 (named M2) were derived from the interpretation of the ETRT by means of the MLS analysis. The comparison between the results of the two models is meant to assess the sensitivity of the numerical model to the layers properties and to validate the outcomes of the MLS analysis. The thermal and hydro-geological parameters assigned to both models are shown in Table 2. For the sake of simplicity, the values implemented layer by layer are not reported here, but an arithmetic mean relative to the main groups of interested lithology (deduced from the stratigraphic log in Figure 3 b) is shown. In addition, the thermal conductivity values and the Darcy velocity values for both models are plotted in Figure 6 and Figure 7 respectively to ease the comparison.

Layer	Model	$k_x=k_y$ (m/s)	θ (-)	K_d (m³/kg)	ρ_b (kg/m³)	Initial_Temp (°C)	D* (m²/s)
Silty sand and	M1	1.20E-04	0.05	1.05E-04	2517.5	15.07	9.67E-06
1-10							
sandy silt	M2	4.59E-04	0.05	2.10E-04	2517.5	15.07	5.76E-06

Fine sand	11-18	M1	2.52E-04	0.07	9.79E-05	2464.5	15.87	6.81E-06
		M2	9.56E-05	0.07	1.96E-04	2464.5	15.87	6.12E-06
Medium sand with gravel	19-31	M1	1.20E-03	0.35	1.79E-04	1722.5	15.40	1.07E-06
		M2	4.48E-04	0.35	1.79E-04	1722.5	15.40	1.33E-06
Clayey silt	32-33	M1	1.00E-08	0.02	1.08E-04	2597.0	15.15	2.47E-05
		M2	1.11E-05	0.02	2.15E-04	2597.0	15.15	1.83E-05
Coarse-medium sand with gravel	34-46	M1	1.20E-03	0.35	1.79E-04	1722.5	15.16	1.07E-06
		M2	5.57E-04	0.35	1.79E-04	1722.5	15.16	1.26E-06
Medium-fine sand	47-63	M1	1.20E-03	0.15	9.56E-05	2252.5	15.02	2.98E-06
		M2	5.23E-04	0.15	1.91E-04	2252.5	15.02	2.44E-06
Silt	56	M1	9.95E-08	0.10	1.00E-04	2385.0	15.01	4.66E-06

Table 2

Hydraulic conductivity, porosity, thermal distribution coefficient, bulk density, initial temperature) and thermal diffusion values implemented in the numerical models M1 and M2

The hydraulic conductivity values along X and Y axis were imposed equals, but along the vertical direction (k_z) the values were divided for 10; these values were derived dividing by the hydraulic gradient the Darcy velocities (Figure 7) achieved from the MLS analysis.

The thermal dispersion process was considered negligible in both models, while the thermal distribution coefficient (depending on solid and water specific heat), the bulk density (depending on solid density and porosity) and the thermal diffusion coefficient (depending on thermal conductivity, porosity, water density and water specific heat) were evaluated according to the equations shown in [13].

Two parameters were used to verify the good fit between the model results and experimental data along the depth for a given time, namely the absolute residual mean error $\widehat{T}_{abs\_res}$ and the root mean squared error RMSE, calculated as follows:

$$\widehat{T}_{abs\_res}(t_k) = \sum_{i=1}^{N} \frac{|T_{meas}(z_i, t_k) - T_{MODFLOW}(z_i, t_k)|}{N} \tag{8}$$

$$RMSE(t_k) = \sqrt{\sum_{i=1}^{N} \frac{[T_{meas}(z_i, t_k) - T_{MODFLOW}(z_i, t_k)]^2}{N}} \tag{9}$$

where T_{meas} is the measured temperature and $T_{MODFLOW}$ is the output temperature of the numerical simulation.

A sensitivity analysis about both hydrogeological properties, by comparing models M1 and M2, and distance between source cell and observation points (U-pipe legs) was carried out and presented in paragraph 3.3.

3. Results

3.1 ILS results

By means of the ILS interpretation the thermal conductivity as function of depth was achieved (Figure 6 in yellow). In specific, in the first 18 meters investigated the thermal conductivity ranges between 1.3 and 2.7 W/(m·K). In this area, layers of silty sand (literature range [66] λ = 1.7 – 5.0 W/(m·K)) and sandy silt (literature range [66] λ = 0.9 – 2.3 W/(m·K)) alternate, therefore the presence of silt brings to a significant decrease of the thermo-physical parameter. The thermal conductivity increases in the following 10 meters, where there is coarse sand (literature range [66] λ = 1.7 – 5.0 W/(m·K)) with gravel (literature value [66] λ = 1.8 W/(m·K)) and it reaches a maximum equal to 3.3 W/(m·K) at 24 m. From 30.5 to 33 m the thermal conductivity decreases because there is a layer of clayey silt, which locally separates the shallow aquifer from the deep aquifer, and after it increases up to 46 m, where a layer of coarse sand is located. In the last 14 meters there is medium-fine sand, except from 51 to 56 m where there is silty sand: the thermal conductivity assumes values similar to those of the first meters investigated.

The values of the thermal conductivity estimated are included within the ranges defined in literature and they follow the lithology very well, i,e. lower values are found in the areas where silty layers are present. Concluding the average heat transfer appears quite similar in the two investigated aquifers as in the local shallow aquifer the mean thermal conductivity value is equal to 2.13 W/(m·K), whereas in the local deep aquifer is equal to 2.10 W/(m·K) (Table 3).
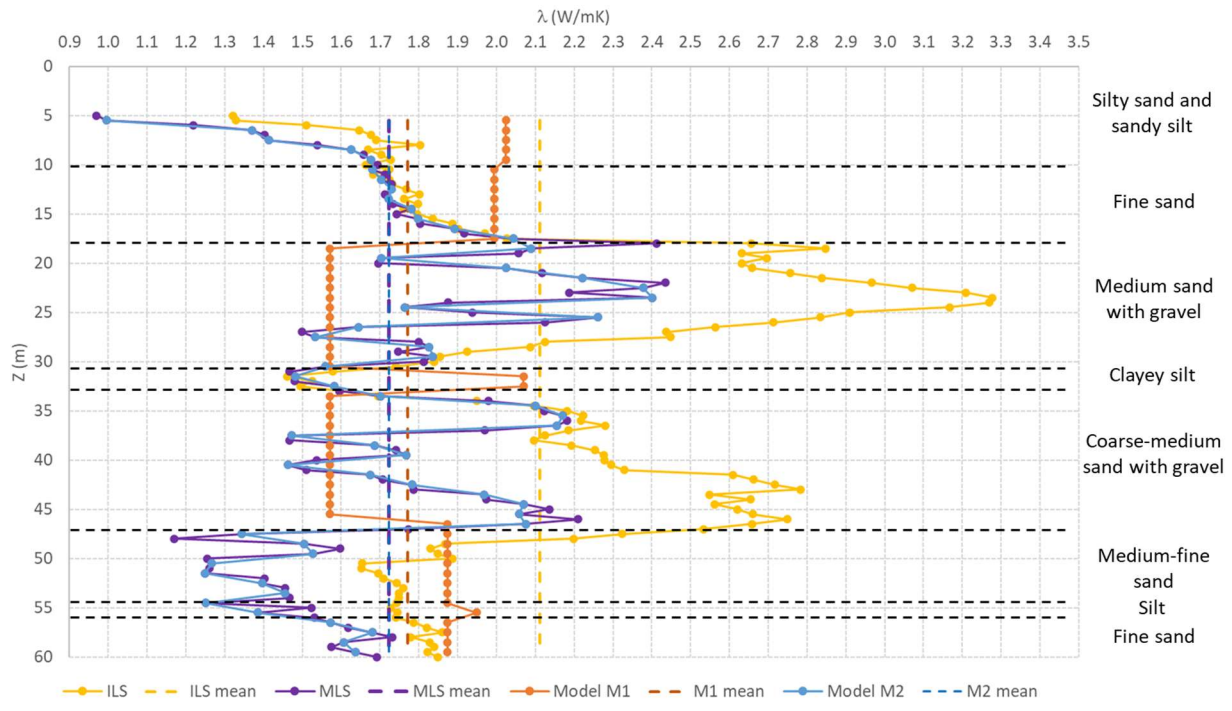
Figure 6 – Thermal conductivity values (continuous lines) as function of depth and mean values (dashed lines) for analytical approaches ILS (yellow plot) and MLS (violet plot) and numerical approaches M1 (orange plot) and M2 (light blue plot).

Parameter	Model	Min	Max	Mean (5-60 m)	Mean - shallow aquifer (5-32.5 m)	Mean – deep aquifer (33-60 m)
λ (W/mK)	ILS	1.32	3.28	2.11	2.13	2.10
	MLS	0.97	2.43	1.72	1.77	1.67
	M1	1.57	2.07	1.77	1.81	1.73
	M2	1.00	2.40	1.72	1.78	1.67
v_D (m/s)	MLS	1.28E-08	3.00E-06	1.30E-06	1.22E-06	1.37E-06
	M1	4.00E-11	4.80E-06	2.74E-06	2.60E-06	2.89E-06
	M2	1.28E-08	3.00E-06	1.28E-06	1.18E-06	1.39E-06

Table 3

Minimum, maximum and mean values of the thermal conductivity (λ) and Darcy velocities (v_D) for analytical solutions (ILS and MLS) and numerical models (M1 and M2).

The results of the parametric analysis are summarized in Table 4. The volumetric thermal capacity spans all the range of variation with an average value of 2.42 MJ/(m^3·K). The source-probe distance varies between 4 cm and 7.5 cm, with an average value of 5.3 cm, meaning that on average the two legs of the U-pipe are almost equally distant from each other and from the borehole border. The mean volumetric heat capacity and the mean source-probe distance values calculated for the shallow aquifer were similar to those found for deep aquifer, as a further proof of the similar lithologies typifying the aquifer. The quality of the fit, represented by the RMSE, varies significantly along the depth. The worst fit (RMSE$_{ILS}$ = 0.39 °C) corresponds to z = 5 m, possibly due to the influence of the outdoor environment, while the best one (RMSE$_{ILS}$ = 0.01 °C) corresponds to z = 29.5 m, the root mean squared error being in general very low in the clayey silt area where conduction is expected to prevail.

Parameter	Model	Min	Max	Mean (5-60 m)	Mean - shallow aquifer (5-32.5 m)	Mean - deep aquifer (33-60 m)
C (MJ/m^3·K)	ILS	2.20	3.40	2.42	2.44	2.39
	MLS	2.20	3.40	2.46	2.43	2.53
r (cm)	ILS	4.0	7.5	5.3	5.0	5.5
	MLS	5.0	8.0	6.2	6.7	6.0
Θ (°)	MLS	0	180	80	65	92
RMSE (°C)	ILS	0.009	0.393	0.072	0.075	0.069
	MLS	0.002	0.021	0.011	0.021	0.017

Table 4

Minimum, maximum and mean values of volumetric heat capacity (C), source-probe distance (r), angle between Darcy velocity and source-probe distance (Θ) and RMSE corresponding to the ILS/MLS fit.

3.2 MLS results

In the silty layers from 5 to 18 meters the thermal conductivity assumes low values and this is consistent with both the literature values and the ILS results (Figure 6). From 18 to 27 meters, the values increase reaching the maximum equal to 2.43 W/(m·K) at 22 m of depth, but in this zone of the shallow aquifer sharp decreases occur at 20 and 27 m. Considering that gravel has a thermal conductivity slightly lower than that of sand, these decreases probably indicate a greater presence of gravel material. The same situation seems to be present also at 36 and 40 m.

In the deep aquifer, until 46 meters of depth the thermal conductivity is similar to the shallow one showing variations due to the gravel abundance. Nevertheless, going down values decrease reaching a local minimum at 50 and 55 m, respectively equal to 1.51 and 1.25 W/(m·K). As for the ILS results, this decrease is justified looking at the stratigraphy (Figure 3a), according to which medium fine sand is located in this zone, with silty layers around 50-56 meters. The thermal conductivity also clearly decreases in correspondence of the clayey silt layer that locally separates the two aquifers at 30.50-33 m.

In general the range of variation of the thermal conductivity obtained with the MLS solution is less wide than that of the ILS solution (Table 3) because the MLS model considers a second parameter, i.e. the Darcy velocity, to evaluate the heat transfer in the soil and to interpret the measured temperature variations. The Darcy velocity were evaluated as the product of the hydraulic gradient and the hydraulic conductivity for each layer concerning numerical models, whereas it was one of the fitting parameters concerning MLS model. Furthermore, it can be noticed that the ILS and the MLS results are similar at depths 5-18 m and 30-35 where the hydraulic conductivity is lower, whereas in all the others layers, where the hydraulic conductivity is higher, the ILS tends to overestimate the thermal conductivity with respect to the MLS. This is also shown by the mean values, being 1.72 W/(m·K) and 2.11 W/(m·K) according to the MLS and the ILS respectively (Table 3).

As far as the Darcy velocity is concerned, Figure 7 shows that the range of values is very wide, from 10^{-8} to $3 \cdot 10^{-6}$ m/s, with a mean velocity equal to $1.3 \cdot 10^{-6}$ m/s. From 5 to 18 m the lithology changes rapidly, alternating silty sand and sandy silt, which has a Darcy velocity lower than the sand. For this reason, the velocity has a very variable trend, with values included between $9.5 \cdot 10^{-8}$ and $2.5 \cdot 10^{-6}$ m/s. Subsequently, from 18 to 29 m coarse sand with gravel is present and the velocity increases reaching the highest values at 20, 24.5 and 27 m (the maximum being $3 \cdot 10^{-6}$ m/s). At 29 m there is a decrease due to the presence of 1 m of weakly silty fine sand and from 30 to 33 m of clayey silt layer. In this area as expected, the velocity reaches the minimum value, equal to $1.3 \cdot 10^{-8}$ m/s at 31.5 m. Entering in the deep aquifer the velocity starts to increase, even if there are two minimum values at 36 and 39 m. In this area, there is coarse sand with gravel, so probably these two decreases are due to a minor presence of gravel. From 40 m the velocity starts to decrease due to the presence of medium-fine sand. The two maximum values at 48 and 50 m, in correspondence of medium sand, could be index of the presence of gravel. From 45.5 to 60 m a layer of medium-fine sand is located, weakly silty from 51 to 56 m, where the velocity decreases.

Concluding, in the silty layers the values of velocity are always lower than those where there is sand with gravel and the abundance of the latter influence the highest values. But in general, the two aquifers show similar Darcy velocities as the shallow aquifer and the deep one have a mean Darcy velocity equal to $1.3 \cdot 10^{-6}$ m/s and $1.4 \cdot 10^{-6}$ m/s respectively (Table 4). By looking at Figure 6 and Figure 7 together, it can be remarked that the regions where the ILS and the MLS predictions

of the thermal conductivity are more different are those where the Darcy velocity, according to the MLS and to the stratigraphy, is larger. This confirms the general idea that, whenever a groundwater flow is present, analysing the TRT with the ILS model somehow turns advection into conduction, leading in an increased effective thermal conductivity.
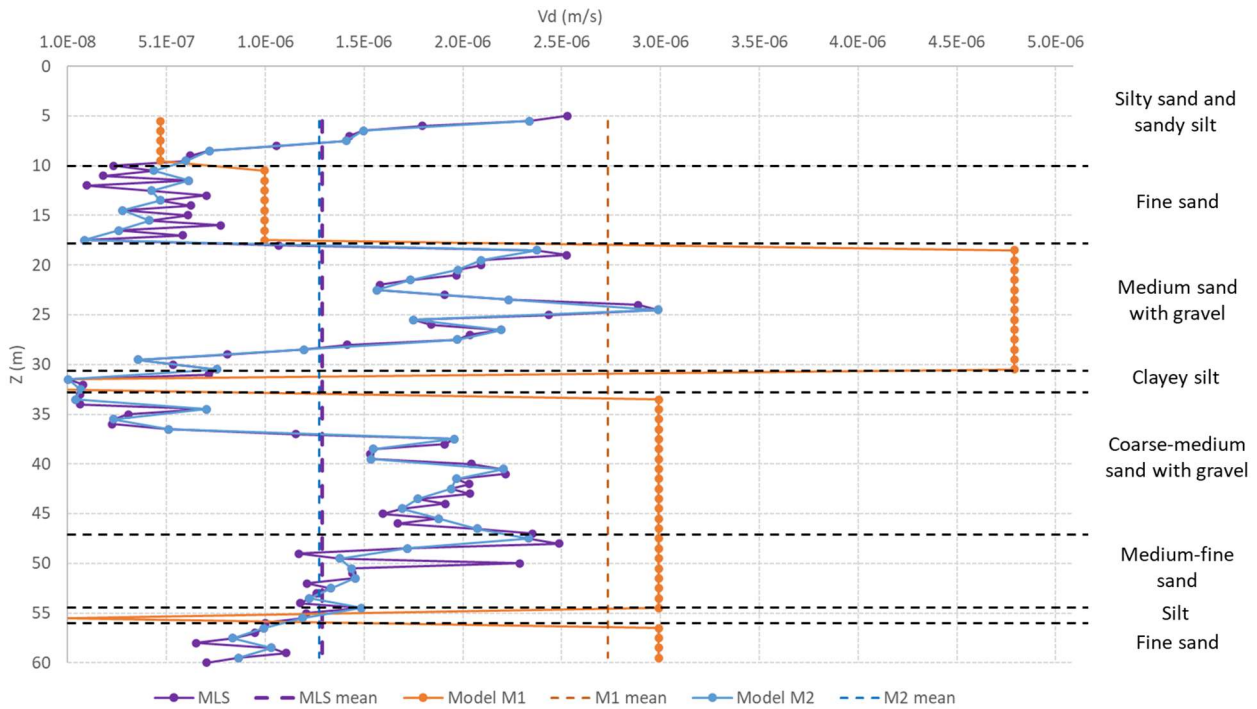

Figure 7 – Darcy velocity values as function of depth (continuous lines) and mean values (dashed lines) for analytical approach MLS (violet plot) and numerical approaches M1 (orange plot) and M2 (light blue plot).

The results of the parametric analysis are shown in Table 4. As far as volumetric thermal capacity and source-probe distance are concerned, the outcomes of the MLS analysis are similar to the ones of the ILS analysis. Regarding the angle between the groundwater velocity and the line joining the U-pipe legs, which is obviously relevant only for the MLS analysis, the mean groundwater flow direction was estimated equal to 80°. It has to be mentioned, however, that the sensitivity to the angle generally appeared small compared to the sensitivity to the thermal capacity and to the source-probe distance.

Considering the RMSE (Table 4), it can be noticed that the MLS solution generally better interprets the TRT data because it also considers the groundwater flow, present in the case study area.

It can be interesting to look back at the ETRT experimental results reported in Figure 4, regarding the temperature increase with time at some depths in the ground, in the light of the outcomes of the MLS analysis. At $z = 25$ m the temperature response is the fastest and the final increase is the lowest. In turn, at $z = 32$ m the temperature response is the slowest and the final increase is the larger. The behaviour at $z = 37$ m is somehow in between. Indeed at $z = 25$ m the thermal

conductivity is found to be 1.94 W/(m·K), namely similar to z = 37 m (λ = 1.97 W/(m·K)) and larger than at z = 32 m (λ = 1.48 W/(m·K)), and at the same time the groundwater velocity is the highest (v_D = 2.4 ·10^{-6} m/s compared to 1.16 ·10^{-6} m/s at z = 37 m and to 8.6 ·10^{-8} m/s at z = 32 m). Therefore, the depth z = 25 m benefits from both effective conduction and advection, the depth z = 32 m is affected by relatively poor conduction and negligible advection and finally at z = 37 m conduction heat transfer is similar to z = 25 m yet advection is less effective.

3.3 MODFLOW/MT3DMS results

A steady state simulation of the groundwater flow reproduced the groundwater flow direction evaluated on site and then the two numerical transport simulations M1 and M2 were run in a transient regime using a stress period 4 days long. For the heat transport simulations, the ITYPE 15 boundary condition allows the injection of energy without circulation of the fluid inside the BHE, such as the ETRT executed with the GEOsniff system. The injection energy q_sT_s assigned to the source cell reproducing the heat cable (cell side of 0.44 cm) was defined as in equation (7) being equal to 3.73·10^{-6} K·m^3/s. The vertical thermal profiles evaluated at three different observation points, located at the distances from the source cell equal to 5, 6.5 and 8 cm, at time t = 96 h are shown in Figure 8 a (model M1) and Figure 8 b (model M2), together with the experimental profile.
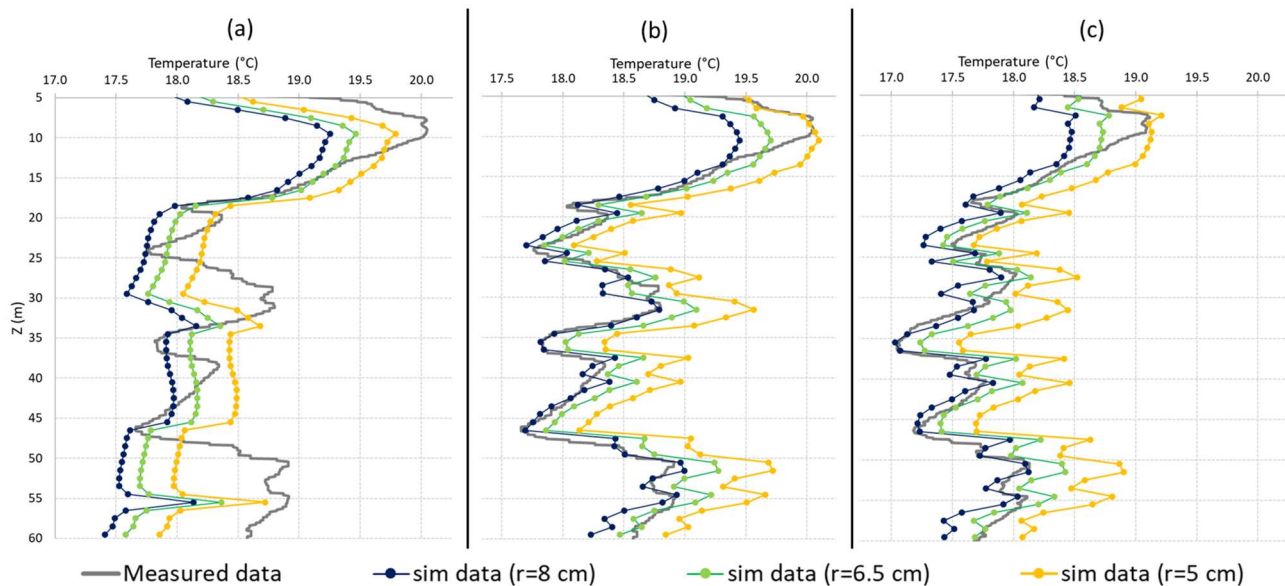

Figure 8 – Temperature distribution along depth for different observation points (blue line for observation point with r=8 cm, green line for 6.5 cm and yellow line for 5 cm) and for (a) output of M1 after a simulation period of 96 h (corresponding to Sensor n.5 release), (b) output of M2 after simulation period of 96 h, (c) output of M2 after simulation period of 24 h (corresponding to Sensor n.4 release).

The simulation results for M1 model after 4 days fit moderately well the experimental data in the three different observation points. The relatively good performance of this model is due to the fact that, as already mentioned in subsection 2.4.3, the ground properties used as input (Table 2) were already optimised in a previous research [61] to reproduce the standard TRT executed on site in 2013. Yet, a residual mean error along the vertical is still present, varying from 0.42 to 0.58 °C depending on the distance, as seen in Table 5. Concerning the RMSE, the observation point located at 5 cm showed the best results, but a difference is still present (0.25 °C).

The model M2 represents an improvement of M1, because is based on detailed hydrogeological and thermal properties resulting from MLS analysis (Table 2). The model M2 results better agree with the experimental data than M1, as demonstrated by the lower absolute residual mean error (varying between 0.2 °C and 0.23 °C) and RMSE (varying in the range 0.15 °C - 0.20 °C) found out along the BHE depth (Table 5). In this case the simulated temperature log at 5 cm from the source is the most distant from experimental data, and the most appropriate distance appears to be 8 cm.

	r = 8 cm			r = 6.5 cm			r = 5 cm		
model	M1	M2	M2	M1	M2	M2	M1	M2	M2
t (h)	96	96	24	96	96	24	96	96	24
$\hat{T}_{abs\_res}$ *(°C)*	0.58	0.20	0.21	0.47	0.23	0.19	0.42	0.47	0.45
RMSE (°C)	0.45	0.20	0.17	0.39	0.15	0.13	0.25	0.25	0.24

Table 5

Residual mean error and root mean squared error for the numerical simulations with models M1 and M2 at different times and distances from the source.

As a further verification of the best performance of model M2 with respect to model M1, the temperature distribution in the aquifer after 24 hours from the turning on of the heating cable was extracted and compared with the experimental temperature measurements (Figure 8 c). Even in this case, the graphs and the statistics (Table 5) allow to state that the numerical heat transport model M2 fits well the experimental data, with an optimal distance from the source of 6.5 cm where the absolute residual mean error is equal to 0.19 °C and the RMSE is 0.13 °C.

By considering the results at both 24 h and 96 h, it may be inferred that the source-probe distance lies between 6.5 cm and 8 cm, which is reasonably in accordance with the MLS results (Table 4), locating the distance between source cell and monitoring point at 6 cm.

4. Discussion

In the given case study, where groundwater flow is present yet the velocity is likely to be moderate, it was found that applying the ILS model to an ETRT apparently leads to acceptable results, in the sense that the local root mean squared error is within the typical temperature probe accuracy. Yet, observing the mean thermal conductivity along the 60 m depth (dashed vertical lines in Figure 6), clearly the ILS is overestimating this parameter if compared with MLS solution. Overall, the average thermal conductivity (5-60 m, see Table 3) obtained with the ILS is 23% larger than the one obtained by means of the MLS analysis.

More in detail the RMSE variation with depth (Figure 9) shows that the best performance of the MLS fits with respect to the ILS is remarkable in most of the ground layers. The fit quality for the two analytical models is equivalent only between 5 m and 18 m and then between 28 m and 37 m, namely in the aquifer regions with low permeable materials where conduction is expected to dominate. Coherently in those regions the thermal conductivity values estimated with the two analytical solutions are very similar (Figure 10 (a)) as the Darcy velocity estimated by the MLS application is very low, as shown in Figure 10 (b). However, these observations alone are not sufficient to state the correctness of the MLS results, therefore a further confirmation was sought by means of the numerical simulations. The comparison of the M1 and M2 simulations shows that implementing the ground thermal and hydrogeological properties derived by the MLS interpretation of the ETRT in a layered numerical model, allows to reproduce very well the measured vertical profiles, providing thus a validation of the MLS approach.

With respect to previous studies applying the MLS to the standard TRT, in this paper the heterogeneity of the subsoil is taken into account and quantified. As far as thermal conductivity is concerned, the variation along the vertical axis is relevant, since the ratio between the maximum (2.43 W/(m·K)) and the minimum value (0.97 W/(m·K)) is equal to 2.5 (Table 3). The Darcy velocity variation along the vertical is even more important, since the ratio between maximum and minimum velocity is found to be 234 (Table 3). If we state that when the Darcy velocity is larger than 10^{-6} m/s the groundwater flow is relevant to heat transfer, following the results in [8], it can be remarked that in this case the BHE is affected by a relevant groundwater flow for about 2/3 of its length (Figure 10 (c)).
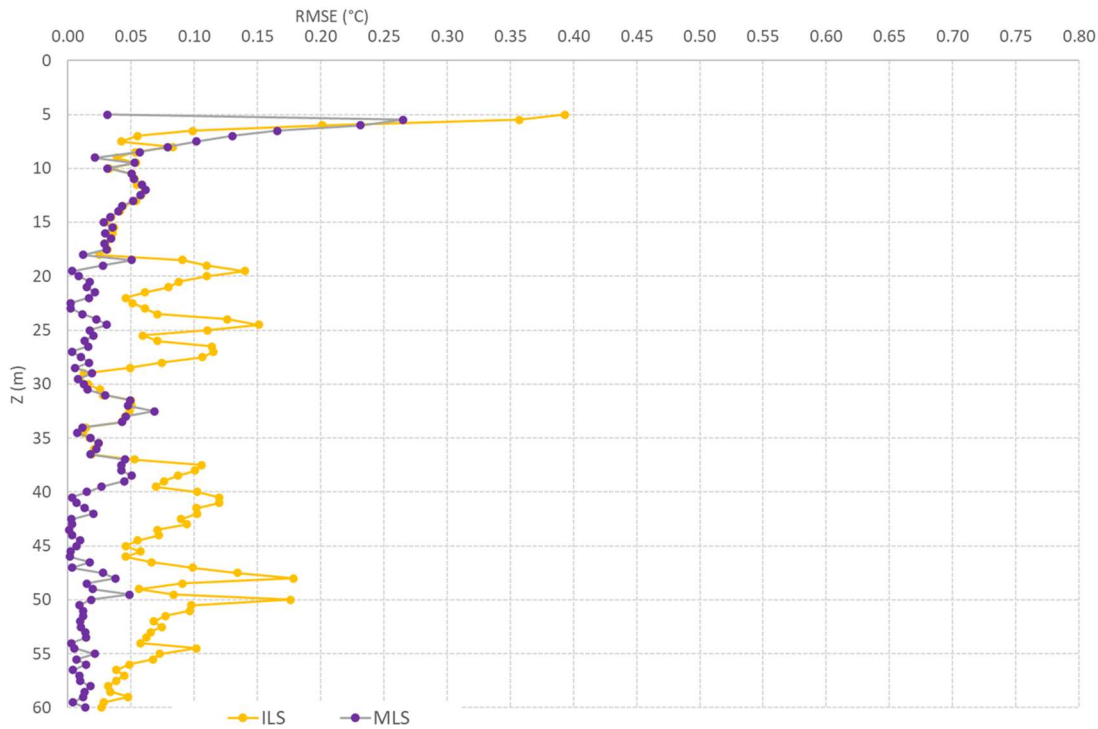
Figure 9 – Temperature root mean squared error for the ILS (yellow plot) and MLS (violet plot) analysis versus depth.

This study also allowed to validate the use of the ITYPE 15 boundary condition in MT3DMS, showing the advantages. In specific, as long as the objective is to simulate a BHE operating at constant heat rate, such as typically during a TRT, there is no longer the need to describe in detail the U-pipe and the thermal carrier fluid by means of tiny cells as it was done in [8]. The pipe can be effectively simulated as a single thermal source cell having the heating cable dimension. This way it is possible to easily implement a numerical model in MT3DMS, saving time and computational burdens.

Operationally, when an ETRT is carried out, if the hydrogeological conditions are known and the groundwater flow is expected to be negligible, the use of the ILS to infer the ground thermal properties can be applied; otherwise if a groundwater flow is present, the use of the MLS is the best choice. Compared to interpreting the ETRT with a layered numerical model, requiring to perform parameter estimation on many parameters for each layer, the MLS represents a simpler and faster approach. Clearly a numerical modelling is more accurate and is a good choice when it is necessary to assess the GSHP system environmental impact through different simulations able to verify the thermal perturbation in the aquifers and forecast possible dangerous temperature increase, thermal interferences between BHEs, or between different GSHP. In those cases, the implementation of an ETRT is strongly suggested. The great advantage of combining an ETRT with the MLS analysis is thus to infer the lithology layering and the corresponding properties, especially in a site where a detailed geognostic survey is not available. That information can be transferred in a groundwater model improving its capacity in simulating the temperature perturbation in the involved aquifers.

At the same time, some limitations of the present research can be identified as follows:

- first of all, the MLS results regarding the groundwater flow direction can be considered only approximate. This depends on the fact that detecting the flow direction by measuring the temperature perturbation in only one point on the horizontal plane is probably insufficient. For research purposes, it could be interesting to apply the MLS approach to a depth-resolved TRT where a temperature distribution around the heat source is measured, such as [48];

- secondly, dealing with a previously realized BHE in this case led to the uncertainty on the distance between the two legs of the U-pipe and to the possibility that it varies along the depth. This problem was faced in this case by performing a parametric analysis on the source-probe distance. However, when planning in the future this kind of ETRT on a custom realized BHE, it might be useful to set a constant distance among the U-pipe branches by using proper spacers;

- overall, the main limit of the kind of ETRT applied in this paper is the low time resolution, related to the relatively small number of temperature probes used. In order to improve the results it would be suggested to use between 8 and 10 temperature probes so as to improve the temperature profile in time (Figure 4) allowing a better fit of the MLS solution. Alternatively, the use of a fiber optic cable can also improve this aspect, but at the other side the use of this technology requires the cable calibration and to face the issue of signal attenuation.
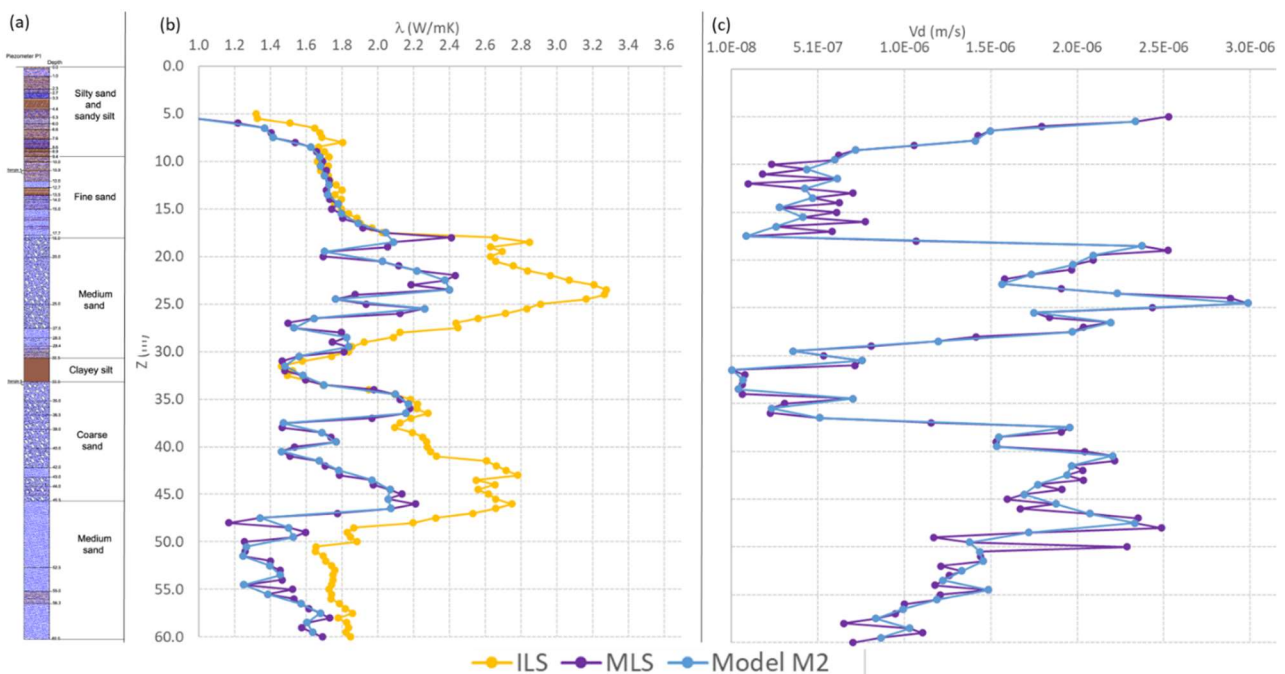

Figure 10 – (a) stratigraphic log of the geognostic survey; (b) thermal conductivity achieved by means of analytical and numerical solutions (ILS yellow line, MLS violet line, Model M2 light blue line); (c) Darcy velocity achieved by means of analytical and numerical solutions (MLS violet line, Model M2 light blue line).

5. Conclusions

In this paper for the first time a depth-resolved Thermal Response Test, specifically an ETRT, is analysed by means of the Moving Line Source model to identify the thermal conductivity and the Darcy velocity distribution along the vertical, in a site where a detailed stratigraphic log was available. According to this approach, it was found that the thermal conductivity ranges between 0.97 W/(m·K) and 2.43 W/(m·K) with an average value of 1.72 W/(m·K), while Darcy velocity lies between $1.28 \cdot 10^{-8}$ m/s and $3.0 \cdot 10^{-6}$ m/s with an average value of $1.3 \cdot 10^{-6}$ m/s. A very good coherence was found between the distribution of the thermal properties and the stratigraphic log.

To test this approach, a comparison was firstly carried out with the Infinite Line Source model, showing that in those regions of the subsoil where conduction is likely to prevail, the ILS and MLS fit equally well and estimate very similar values of the thermal conductivity. In turn, in those regions where groundwater flow is significant, the quality of the ILS interpolation is poorer and the effect of the advection are poured into a higher effective thermal conductivity, which is overestimated with respect to the pure thermal conductivity obtained by the MLS fit by 23%. The capability of the MLS to correctly identify both the thermal conductivity and the groundwater velocity in those regions was demonstrated by the numerical simulations performed in MODFLOW/MT3DMS on a layered model, featuring the thermal and hydrogeological properties of each lithography derived from the MLS analysis. Moreover, it was verified that the ITYPE 15 boundary condition, that encompasses the modelling of the pipe as a heat source, is the best choice in MODFLOW/MT3DMS to effectively simulate a TRT, avoiding the detailed description of the U-pipe.

This study allowed at the same time to identify the intrinsic low sensitivity of the procedure to the groundwater direction and the main limitations of the combined ETRT/MLS approach proposed, namely the low time resolution of the test and the uncertainty on the distance between the two legs in the test BHE. Suggestions about how to overcome these limitations were provided.

The potential of the combined ETRT/MLS approach is the possibility to perform an accurate design of the GSHP system, taking into account the variability of the ground thermal properties along the BHE depth as well as the presence, the thickness and the velocity of the aquifer encountered along it. In the given case study, it was found that 2/3 of the BHE extension are invested by a significant groundwater flow and thus are likely to exhibit a larger heat exchange rate compared to the remaining portion. The outcomes of the combined ETRT/MLS approach could be implemented either in a layered numerical model or in a proper design methodology such as [56], able to take into account multiple ground layers and groundwater flow. The detailed knowledge of the heat transfer potential along the depth will avoid both oversizing of the BHE, which increases the capital cost of the GSHP largely influenced by the excavation cost and undersizing of the BHE, which compromises the sustainable operation of the GSHP in the long-term as well as the heat

pump energy efficiency. Furthermore, the improvement in the aquifers properties knowledge will enhance the assessment of GSHP system environmental impact, allowing the correct representation of different plumes and related thermal perturbation in different portions of the hydrogeological system. Consequently, an ETRT is strongly recommended when the aquifer is heterogenous and the size of the GSHP system requires the assessment of thermal perturbation through a numerical model.

References

[1]   Bayer P, Saner D, Bolay S, Rybach L, Blum P. Greenhouse gas emission savings of ground source heat pump systems in Europe: A review. Renew Sustain Energy Rev 2020;16:1256–67. doi:10.1016/j.rser.2011.09.027.

[2]   Lee J. Current status of ground source heat pumps in Korea. Renew Sustain Energy Rev 2009;13:1560–8. doi:10.1016/j.rser.2008.10.005.

[3]   Farabi-asl H, Chapman A, Itaoka K, Noorollahi Y. Ground source heat pump status and supportive energy policies in Japan. Energy Procedia 2019;158:3614–9. doi:10.1016/j.egypro.2019.01.902.

[4]   Cetin A, Kagan Y, Paksoy H. Underground thermal heat storage and ground source heat pump activities in Turkey. Sol Energy 2020;200:22–8. doi:10.1016/j.solener.2018.12.055.

[5]   Roy D, Chakraborty T, Basu D, Bhattacharjee B. Feasibility and performance of ground source heat pump systems for commercial applications in tropical and subtropical climates. Renew Energy 2020;152:467–83. doi:10.1016/j.renene.2020.01.058.

[6]   Bear J. Dynamics of Fluids in Porous Media. New York: Dover; 1972.

[7]   Fujii H, Itoi R, Fujii J, Uchida Y. Optimizing the design of large-scale ground-coupled heat pump systems using groundwater and heat transport modeling. Geothermics 2005;34:347–64. doi:10.1016/j.geothermics.2005.04.001.

[8]   Angelotti A, Alberti L, La Licata I, Antelmi M. Energy performance and thermal impact of a Borehole Heat Exchanger in a sandy aquifer: Influence of the groundwater velocity. Energy Convers Manag 2014;77:700–8. doi:10.1016/j.enconman.2013.10.018.

[9]   Chiasson AD, Rees SJ, Spitler JD. Preliminary assessment of the effects of groundwater flow on closed-loop ground-source heat pump systems. ASHRAE Trans 2000;106:380–93.

[10]   Fujii H, Inatomi T, Itoi R, Uchida Y. Development of suitability maps for ground-coupled heat pump systems using groundwater and heat transport models. Geothermics 2007;36:459–72. doi:10.1016/j.geothermics.2007.06.002.

[11]   Fan R, Jiang Y, Yao Y, Shiming D, Ma Z. A study on the performance of a geothermal heat exchanger under coupled heat conduction and groundwater advection. Energy 2007;32:2199–209. doi:10.1016/j.energy.2007.05.001.

[12]   Hein P, Kolditz O, Görke U, Bucher A, Shao H. A numerical study on the sustainability and efficiency of borehole heat exchanger coupled ground source heat pump systems. Appl Therm Eng 2016;100:421–33. doi:10.1016/j.applthermaleng.2016.02.039.

[13]   Alberti L, Angelotti A, Antelmi M, La Licata I. A numerical study on the impact of grouting material on borehole heat exchangers performance in aquifers. Energies 2017;10. doi:10.3390/en10050703.

[14]   You T, Wang B, Li X, Shi W, Yang H. A general distributed parameter model for ground heat exchangers with arbitrary shape and type of heat sources. Energy Convers Manag 2018;164:667–79. doi:10.1016/j.enconman.2018.03.059.

[15]   Attard G, Bayer P, Rossier Y, Blum P, Eisenlohr L. A novel concept for managing thermal interference between geothermal systems in cities. Renew Energy 2020;145:914–24. doi:10.1016/j.renene.2019.06.095.

[16]   Hecht-Méndez J, de Paly M, Beck M, Bayer P. Optimization of energy extraction for vertical closed-loop geothermal systems considering groundwater flow. Energy Convers Manag 2013;66:1–10. doi:10.1016/j.enconman.2012.09.019.

[17]   Rivera JA, Blum P, Bayer P. Analytical simulation of groundwater flow and land surface effects on thermal plumes of borehole heat exchangers. Appl Energy 2015;146:421–33. doi:10.1016/j.apenergy.2015.02.035.

[18]   Wang H, Qi C, Du H, Gu J. Thermal performance of borehole heat exchanger under groundwater flow: A case study from Baoding. Energy Build 2009;41:1368–73. doi:10.1016/j.enbuild.2009.08.001.

[19]   Casasso A, Sethi R. Efficiency of closed loop geothermal heat pumps: A sensitivity analysis. Renew Energy 2014;62:737–46. doi:10.1016/j.renene.2013.08.019.

[20]   Samson M, Dallaire J, Gosselin L. Influence of groundwater flow on cost minimization of ground coupled heat pump systems. Geothermics 2018;73:100–10. doi:10.1016/j.geothermics.2018.01.003.

[21]   Tang F, Nowamooz H. Long-term performance of a shallow borehole heat exchanger installed in a geothermal field of Alsace region. Renew Energy 2018;128:210–22. doi:10.1016/j.renene.2018.05.073.

[22]   Moradi A, Smits KM, Massey J, Cihan A, Mccartney J. Impact of coupled heat transfer and water flow on soil borehole thermal energy storage (SBTES) systems: Experimental and modeling investigation. Geothermics 2015;57:56–72. doi:10.1016/j.geothermics.2015.05.007.

[23]   Capozza A, Carli M De, Zarrella A. Investigations on the influence of aquifers on the ground temperature in ground-source heat pump operation. Appl Energy 2013;107:350–63. doi:10.1016/j.apenergy.2013.02.043.

[24]   Rivera JA, Blum P, Bayer P. Ground energy balance for borehole heat exchangers: Vertical fluxes, groundwater and storage. Renew Energy 2015;83:1341–51. doi:10.1016/j.renene.2015.05.051.

[25]   Bucci A, De Luca D, Lasagna M, Malandrino M. Impacts of borehole heat exchangers (BHEs) on groundwater quality: the role of heat-carrier fluid and borehole grouting. Environ Earth Sci 2018;77:175. doi:10.1007/s12665-018-7375-9.

[26]   Mogensen P. Fluid to duct wall heat transfer in duct system heat storage. Proc Int Conf Surf Heat Storage Theory Pract 1983:657–657.

[27]   Austin WA, Yavuzturk C, Spitler JD. Development of an In-Situ System and Analysis Procedure for Measuring Ground Thermal Properties. ASHRAE Trans 2000;106:365–79.

[28]   Gehlin S. Thermal Response Test. Method Development and Evaluation. Luleå Univ Technol 2002:191.

[29]   Witte H, Van Gelder G, Spitler J. In Situ Measurement of Ground Thermal Conductivity: A Dutch Perspective. ASHRAE Trans 2002;108.

[30]   Zhang C, Guo Z, Liu Y, Cong X, Peng D. A review on thermal response test of ground-coupled heat pump systems. Renew Sustain Energy Rev 2014;40:851–67. doi:10.1016/j.rser.2014.08.018.

[31]   Spitler JD, Gehlin SEA. Thermal response testing for ground source heat pump systems—An historical review. Renew Sustain Energy Rev 2015;50:1125–37. doi:10.1016/j.rser.2015.05.061.

[32]   Naldi C, Zanchini E. Full-Time-Scale Fluid-to-Ground Thermal Response of a Borefield with Uniform Fluid Temperature. Energies 2019;12. doi:10.3390/en12193750.

[33]   Carlslaw H., Jaeger JC. Heat conduction in solids. Oxford University Press; 1959.

[34]   Witte HJL. Geothermal Response Tests with Heat Extraction and Heat Injection: Examples of Application in Research and Design of. Worskhop Eur. sur Test Reponse Geotherm., vol. 31, Lausanne: 2001.

[35]   Signorelli S, Bassetti S, Pahud D, Kohl T. Numerical evaluation of thermal response tests. Geothermics 2007;36:141–66. doi:10.1016/j.geothermics.2006.10.006.

[36]   Raymond J, Therrien R, Gosselin L, Lefebvre R. Numerical analysis of thermal response tests with a groundwater fl ow and heat transfer model. Renew Energy 2011;36:315–24. doi:10.1016/j.renene.2010.06.044.

[37]   Tang F, Nowamooz H. Sensitive analysis on the effective soil thermal conductivity of the Thermal Response Test considering various testing times, field conditions and U-pipe lengths. Renew Energy 2019;143:1732–43. doi:10.1016/j.renene.2019.05.120.

[38]   Katsura T, Nagano K, Kindaichi S. Heat trAnsfer experiment in the ground with ground water advection [C]. Proc Ecostock, Stock USA 2006.

[39]   Wagner V, Bayer P, Bisch G, Markus K, Blum P. Hydraulic characterization of aquifers by thermal response

testing: Validation by large-scale tank and field experiments. Water Resour Manag 2014;50:71–85. doi:10.1002/2013WR013939.

[40]   Angelotti A, Molinaroli L. A laboratory apparatus to study thermal response test in the presence of groundwater flow. E3S Web Conf 2019;111. doi:10.1051/e3sconf/201911101067.

[41]   Sutton MG, Nutter DW, Couvillion RJ. A Ground Resistance for Vertical Bore Heat Exchangers With Groundwater Flow. J Energy Resour Technol 2003;125:183–9. doi:10.1115/1.1591203.

[42]   Diao N, Li Q, Fang Z. Heat transfer in ground heat exchangers with groundwater advection. Int J Therm Sci 2004;43:1203–11. doi:10.1016/j.ijthermalsci.2004.04.009.

[43]   Chiasson A, O'Connell A. New analytical solution for sizing vertical borehole ground heat exchangers in environments with significant groundwater flow: Parameter estimation from thermal response test data. HVAC&R Res 2011;1078–9669. doi:10.1080/10789669.2011.609926.

[44]   Wagner V, Blum P, Kübert M, Bayer P. Analytical approach to groundwater-influenced thermal response tests of grouted borehole heat exchangers. Geothermics 2013;46:22–31. doi:10.1016/j.geothermics.2012.10.005.

[45]   Angelotti A, Ly F, Zille A. On the applicability of the moving line source theory to thermal response test under groundwater flow: considerations from real case studies. Geotherm Energy 2018;6. doi:10.1186/s40517-018-0098-z.

[46]   Chae H, Nagano K, Sakata Y, Katsura T, Kondo T. Estimation of fast groundwater flow velocity from thermal response test results. Energy Build 2020;206:109571. doi:10.1016/j.enbuild.2019.109571.

[47]   Rouleau J, Gosselin L. Inverse heat transfer applied to a hydrogeological and thermal response test for geothermal applications. Int J Therm Sci 2016;109:70–80. doi:10.1016/j.ijthermalsci.2016.05.021.

[48]   Michalski A, Klitzsch N. First field application of temperature sensor modules for groundwater flow detection near borehole heat exchanger. Geotherm Energy 2019;7:37. doi:10.1186/s40517-019-0152-5.

[49]   Wilke S, Menberg K, Steger H, Blum P. Advanced thermal response tests: A review. Renew Sustain Energy Rev 2020;119:109575. doi:10.1016/j.rser.2019.109575.

[50]   Acuña J, Mogensen P, Palm B. Distributed thermal response tests on a multi-pipe coaxial borehole heat exchanger. HVAC&R Res 2011;1078–9669. doi:10.1080/10789669.2011.625304.

[51]   Acuña J, Palm B. Distributed thermal response tests on pipe-in-pipe borehole heat exchangers. Appl Energy 2013;109:312–20. doi:10.1016/j.apenergy.2013.01.024.

[52]   Sakata Y, Katsura T, Nagano K. Multilayer-concept thermal response test: Measurement and analysis methodologies with a case study. Geothermics 2018;71:178–86. doi:10.1016/j.geothermics.2017.09.004.

[53]   Martos; J, Montero A, Torres J, Soret J, Martínez G, García-Olcina R. Novel Wireless Sensor System for

Dynamic Characterization of Borehole Heat Exchangers. Sensors 2011;11:7082–94. doi:10.3390/s110707082.

[54] Raymond J, Lamarche L, Malo M. Field demonstration of a first thermal response test with a low power source. Appl Energy 2015;147:30–9. doi:10.1016/j.apenergy.2015.01.117.

[55] Blasi A, Menichetti M. Thermal conductivity distributed from a Thermal Response Test (TRT) in a borehole heat exchanger (BHE). Ital J Groundw 2012:41–8. doi:10.7343/AS-010-12-0027.

[56] Hu J. An improved analytical model for vertical borehole ground heat exchanger with multiple-layer substrates and groundwater flow. Appl Energy 2017;202:537–49. doi:10.1016/j.apenergy.2017.05.152.

[57] Alberti L, Antelmi M, Angelotti A, Formentin G. Geothermal heat pumps for sustainable farm climatization and field irrigation. Agric Water Manag 2018;195. doi:10.1016/j.agwat.2017.10.009.

[58] Bersezio R, Giudici M, Mele M. Combining sedimentological and geophysical data for high-resolution 3-D mapping of fluvial architectural elements in the Quaternary Po plain (Italy). Sediment Geol 2007;202:230–48. doi:10.1016/j.sedgeo.2007.05.002.

[59] Mele M, Bersezio R, Giudici M. Hydrogeophysical imaging of alluvial aquifers: Electrostratigraphic units in the quaternary Po alluvial plain (Italy). Int J Earth Sci 2012;101:2005–25. doi:10.1007/s00531-012-0754-7.

[60] Antelmi M. Modellazione numerica del trasporto di calore in falda per lo studio delle prestazioni energetiche e degli impatti termici derivanti dall'attivita' di una sonda geotermica (in Italian). PHD Thesis 2016:1–282.

[61] Ly F. Interpretation of Borehole Heat Exchangers Thermal Response Tests under groundwater influence: analysis of three case studies. Master Degree Thesis 2015.

[62] Harbaugh AW, Banta ER, Hill MC, McDonald MG. MODFLOW-2000 , The U .S . Geological Survey modular graound-water model — User guide to modularization concepts and the ground-water flow process. US Geol Surv 2000:130.

[63] Zheng C, Wang PP. MT3DMS: A Modular Three-Dimensional Multispecies Transport Model for simulation of advection, dispersion and chemical reactions of contaminants in groundwater systems. Contract Rep SERDP-99-1 1999:239.

[64] Thorne D, Langevin CD, Sukop MC. Addition of simultaneous heat and solute transport and variable fluid viscosity to SEAWAT. Comput Geosci 2006;32:1758–68. doi:10.1016/j.cageo.2006.04.005.

[65] Hecht-Méndez J, Molina-Giraldo N, Blum P, Bayer P. Evaluating MT3DMS for Heat Transport of Closed Geothermal Systems. Ground Water 2010;48:741–56. doi:10.1111/j.1745-6584.2010.00678.x.

[66] Molina-Giraldo N, Bayer P, Blum P. Evaluating the influence of thermal dispersion on temperature plumes from geothermal systems using analytical solutions. Int J Therm Sci 2011;50:1223–31. doi:10.1016/j.ijthermalsci.2011.02.004.